(+/−)-Lucidumone, a COX-2 Inhibitory Caged Fungal Meroterpenoid from *Ganoderma lucidum*

Yong-Ming Yan,[†,#] Hao-Xing Zhang,[†,#] Huan Liu,[†,#] Yan Wang,[‡] Jing-Bo Wu,[†] Yan-Peng Li,[†] and Yong-Xian Cheng*[,†]

[†] School of Pharmaceutical Sciences, Health Science Center, College of Life Sciences and Oceanography, Shenzhen University, Shenzhen 518060, PR China

[‡] Center for Translation Medicine Research and Development, Shenzhen Institute of Advanced Technology, Chinese Academy of Sciences, Shenzhen 518055, PR China

Contents of Supporting Information

Table S1. ^{1}H (600 MHz) and ^{13}C NMR (150 MHz) Data of of **1** in DMSO-d_6 (δ in ppm, J in Hz).

No	δ_H	δ_C	HMBC (H → C)	ROESY
1		148.3		
2		125.2		
3		135.2		
4		147.7		
5	6.97 d (8.6)	124.9	C-1, C-3, C-7′	
6	6.71 d (8.6)	118.1	C-2, C-4	
1′		201.0		
2′	2.70 d (2.2)	61.2	C-1′, C-3′, C-4′, C-7′, C-9′, C-11′	H-4′, H-12′, Hb-10′
3′		51.3		
4′	3.75 brs	77.6		H-2′, H-12′, Hb-10′
5′	2.24 t-like (4.5)	47.8		H-6′
6′	2.55 q-like (3.5)	37.5	C-3, C-2′, C-4′, C-7′	H-5′, Ha-10′
7′		85.3		
8′	Ha 1.71 m	15.5		
	Hb 0.86 m			
9′	Ha 1.99 m	14.8		
	Hb 1.08 m			
10′	Ha 4.05 dd (8.1, 4.8)	72.8	C-4′, C-5′, C-7′	H-5′, H-6′
	Hb 3.64 d (8.1)		C-4′, C-5′, C-7′	H-4′
11′		211.5		
12′	2.16 s	28.1	C-3′, C-11′	H-2′, H-4′

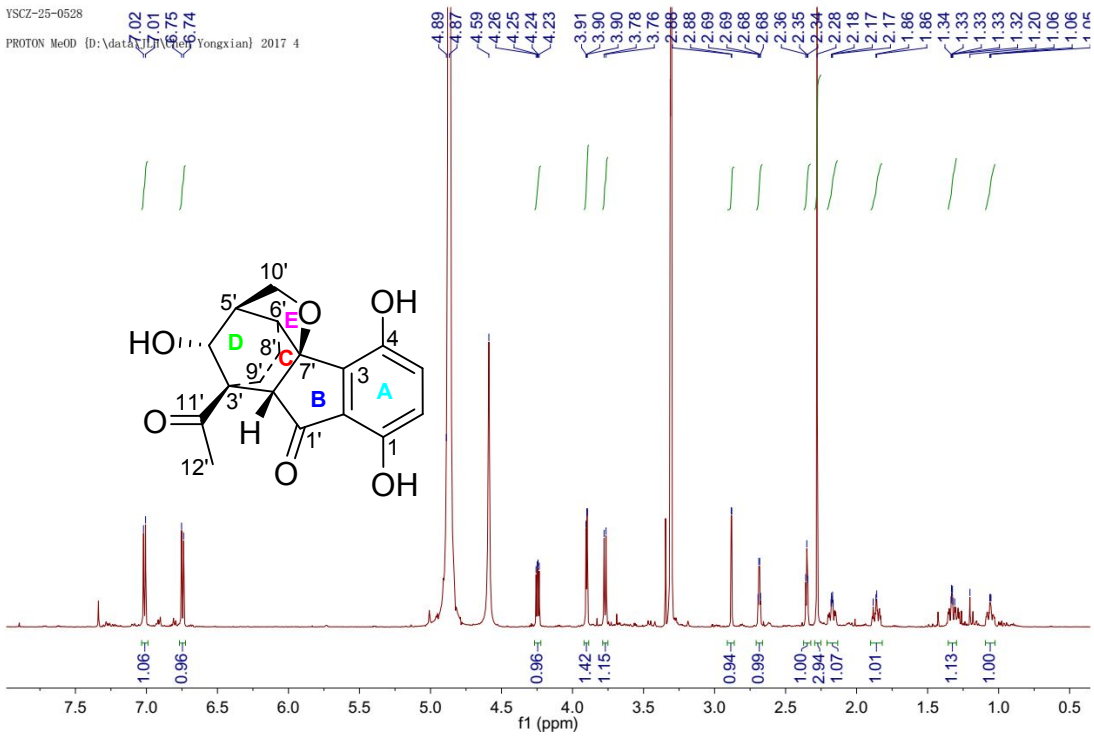

Figure S1. ^{1}H NMR spectrum of **1** in methanol-d_4.

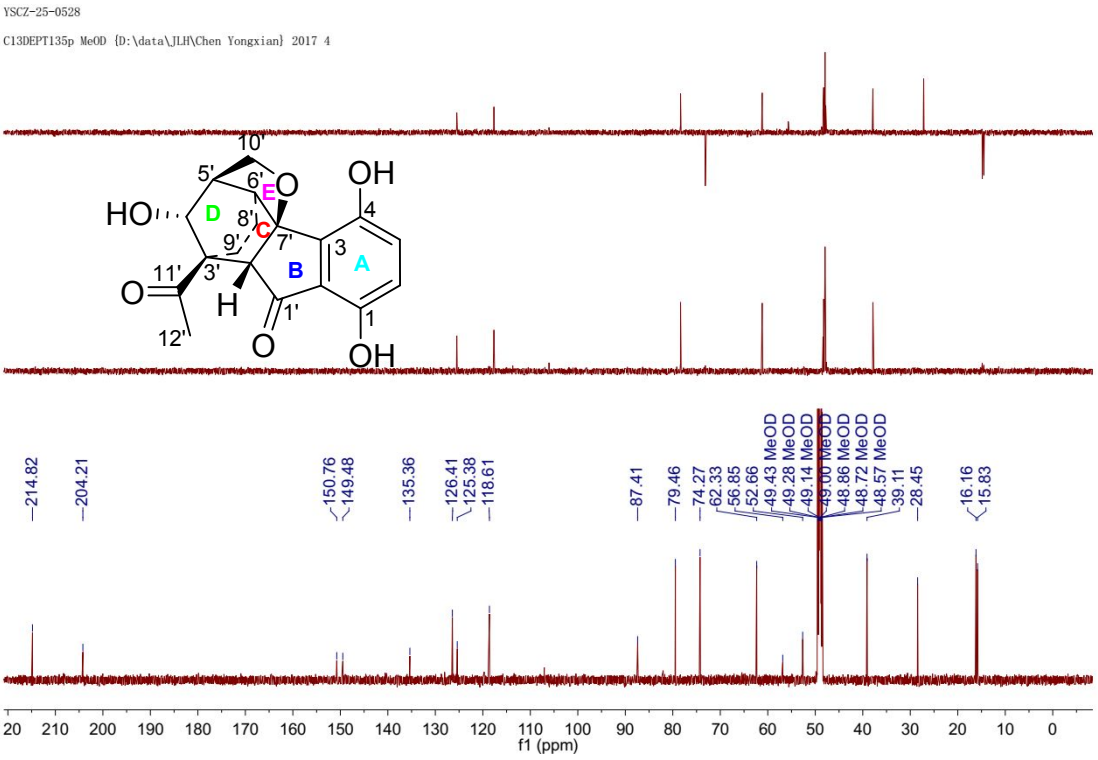

Figure S2. ^{13}C NMR and DEPT spectra of **1** in methanol-d_4.

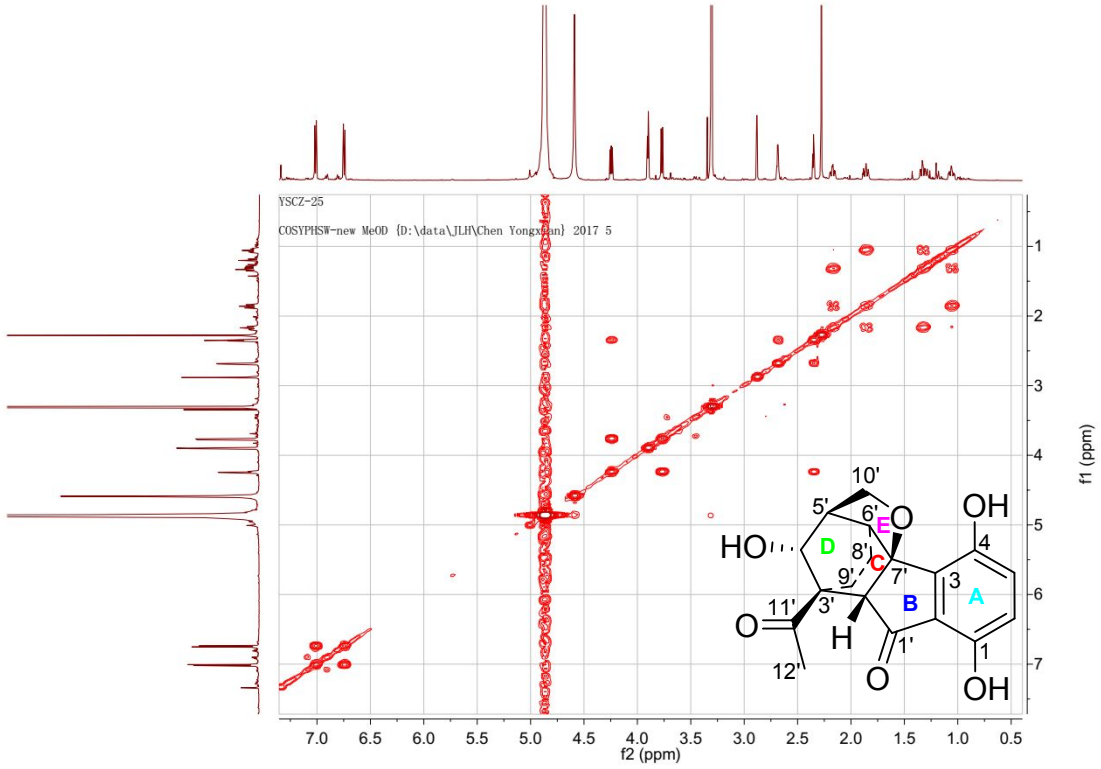

Figure S3. ^{1}H-^{1}H COSY spectrum of **1** in methanol-d_4.

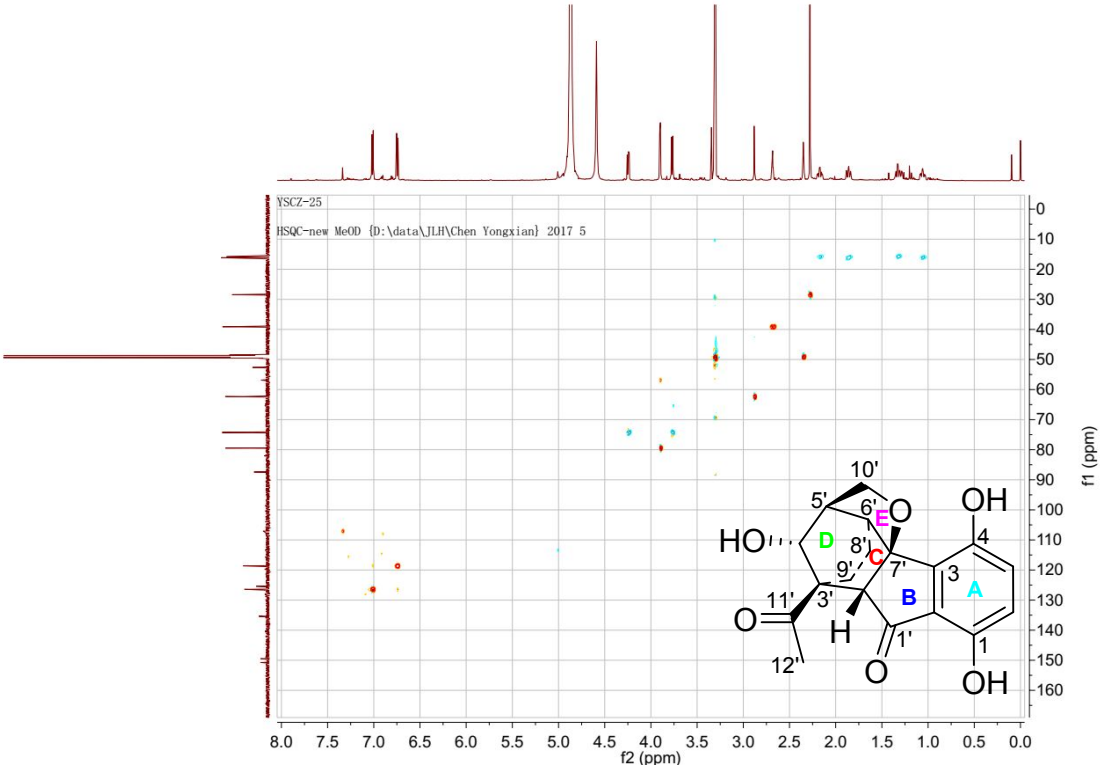

Figure S4. HSQC spectrum of **1** in methanol-d_4.

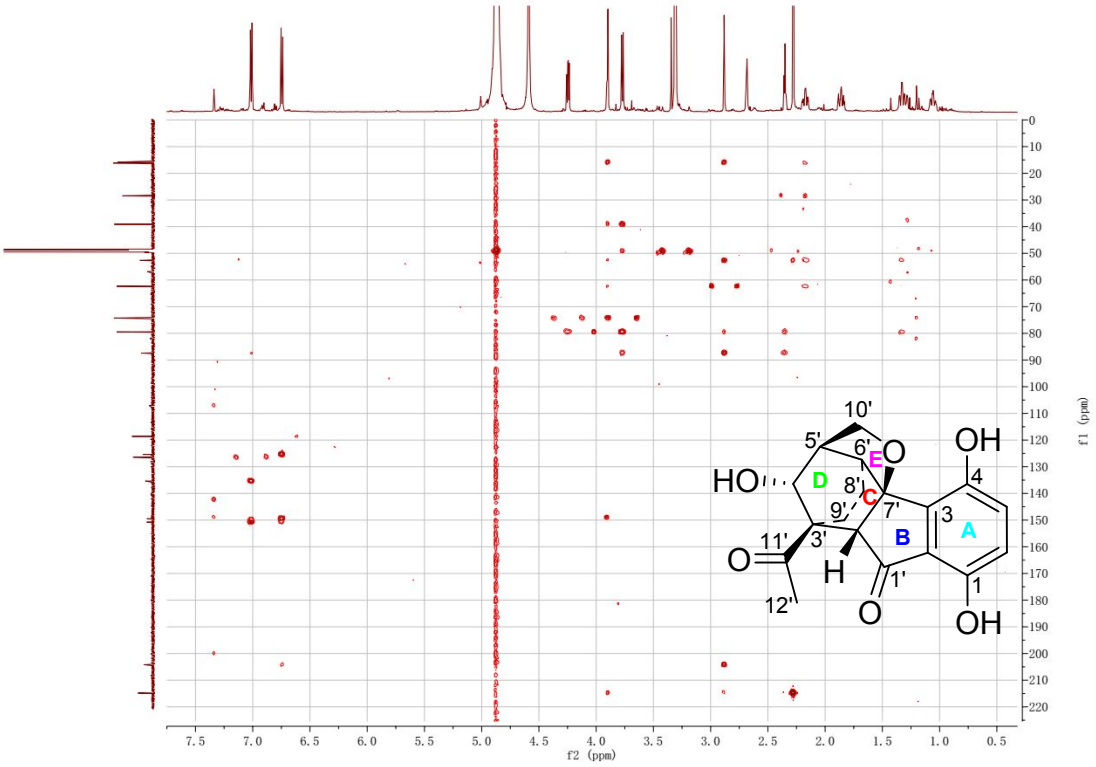

Figure S5. HMBC spectrum of **1** in methanol-d_4.

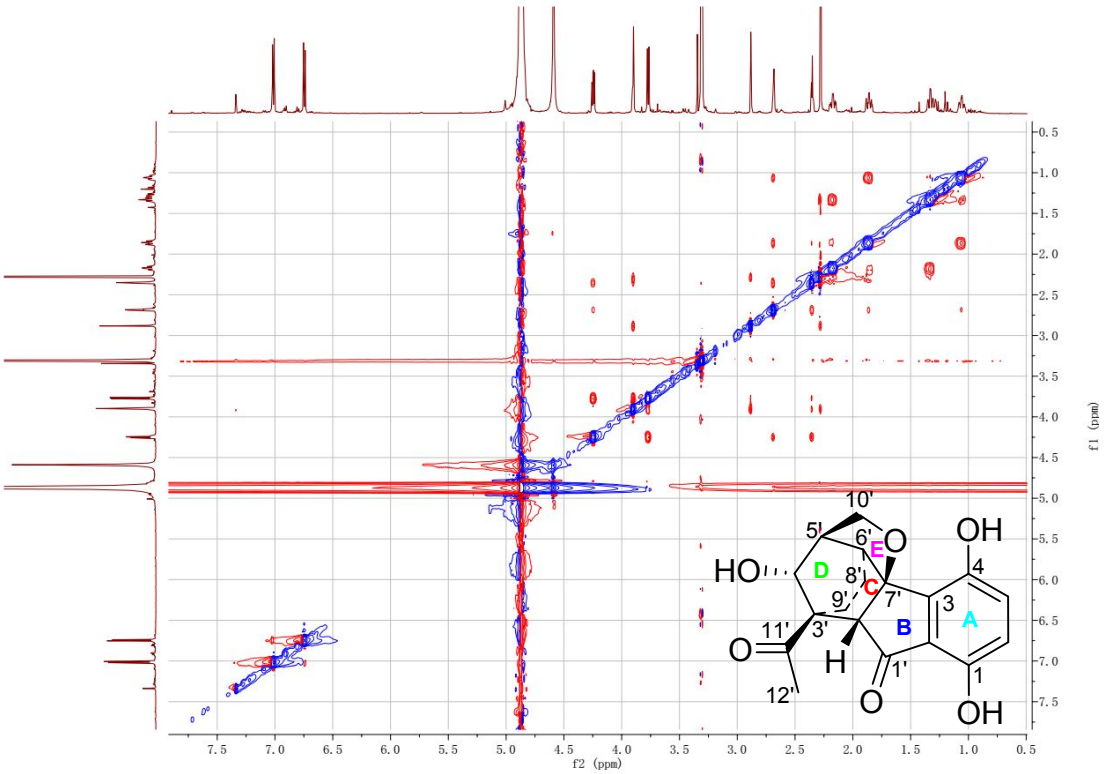

Figure S6. ROESY spectrum of **1** in methanol-d_4.

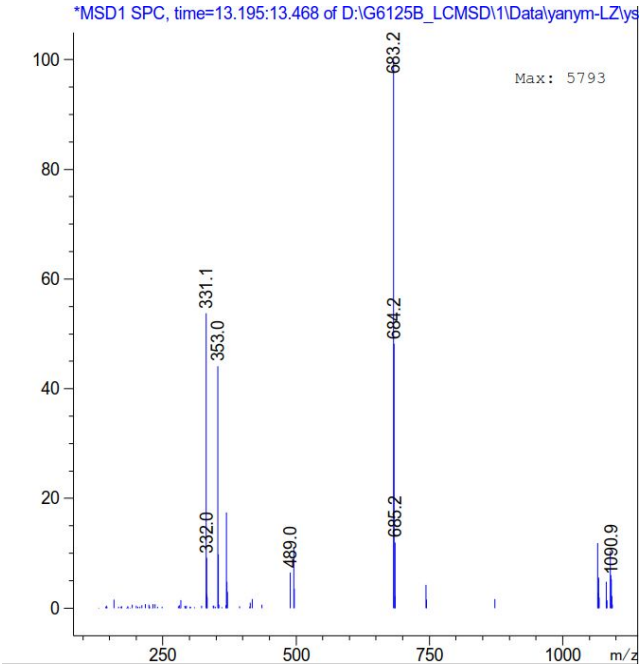

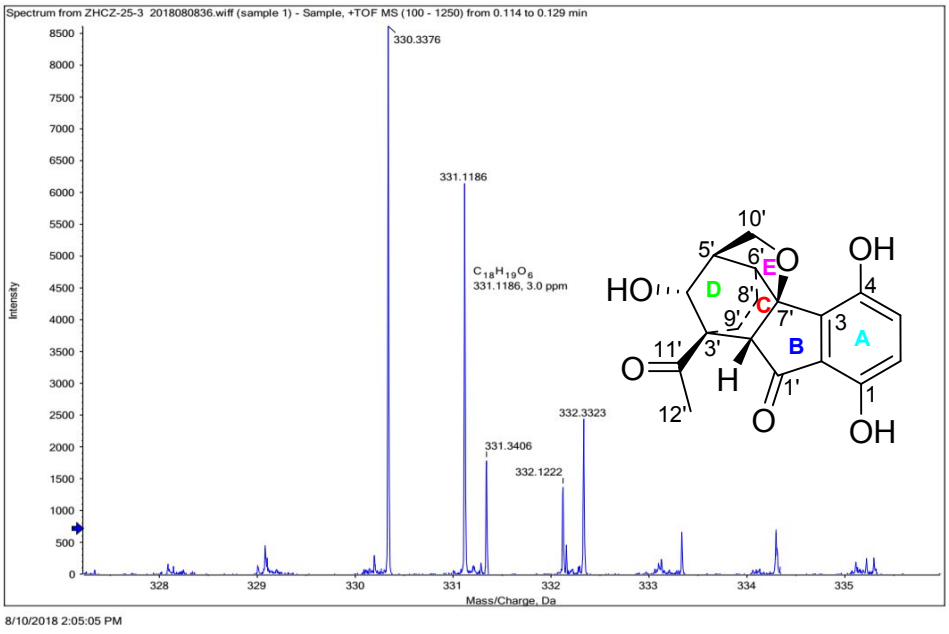

Hit	Formula	m/z	RDB	ppm
1	$C_{18}H_{19}O_6$	331.1176	10.0	3.0

Figure S7. MS and HRESIMS of **1**.

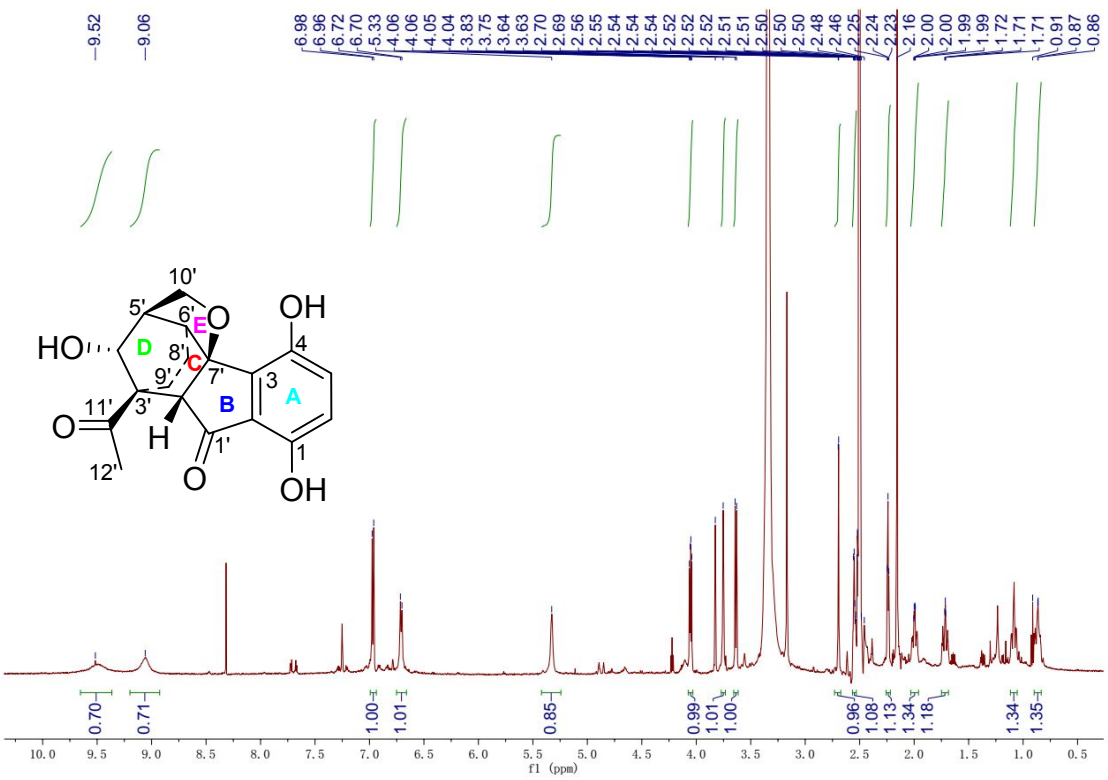

Figure S8. ^{1}H NMR spectrum of **1** in DMSO-d_6.

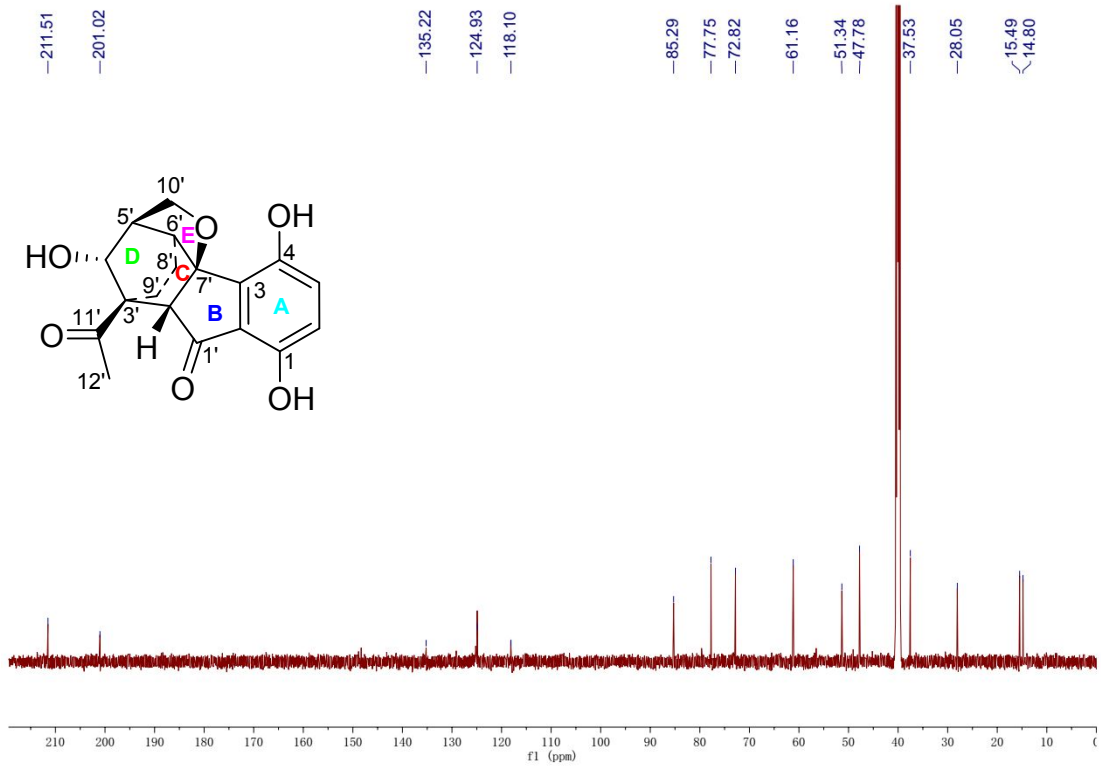

Figure S9. ^{13}C NMR spectrum of **1** in DMSO-d_6.

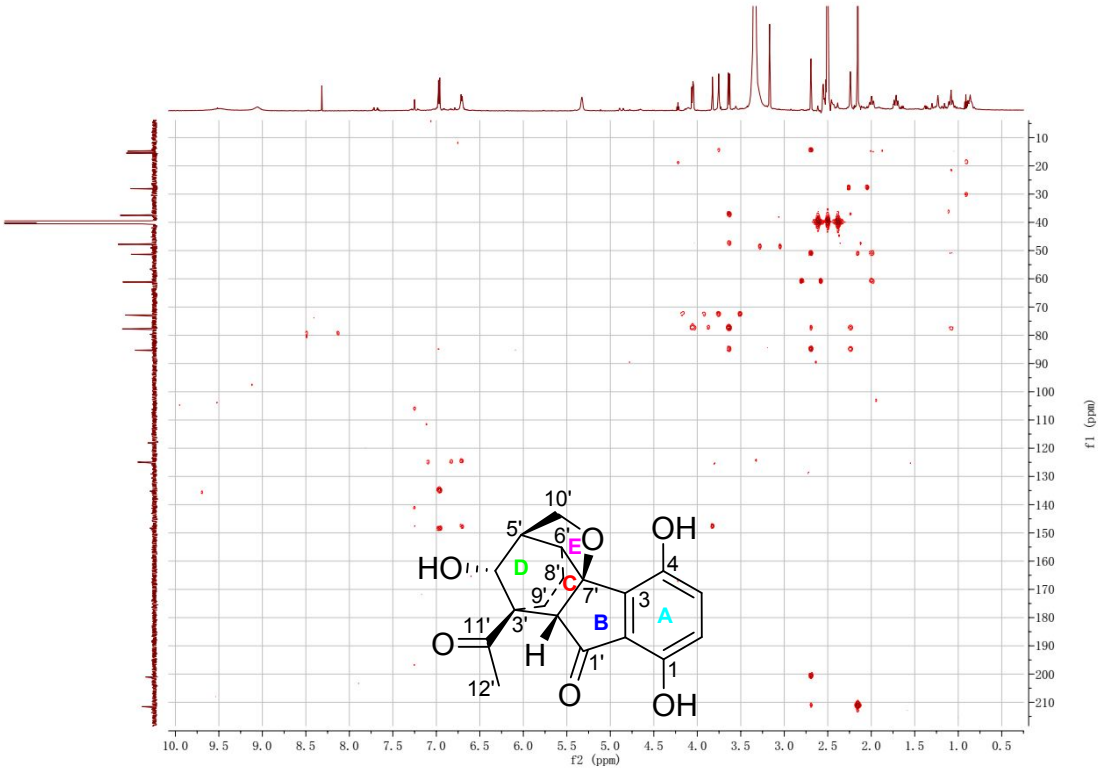

Figure S10. HMBC spectrum of **1** in DMSO-d_6.

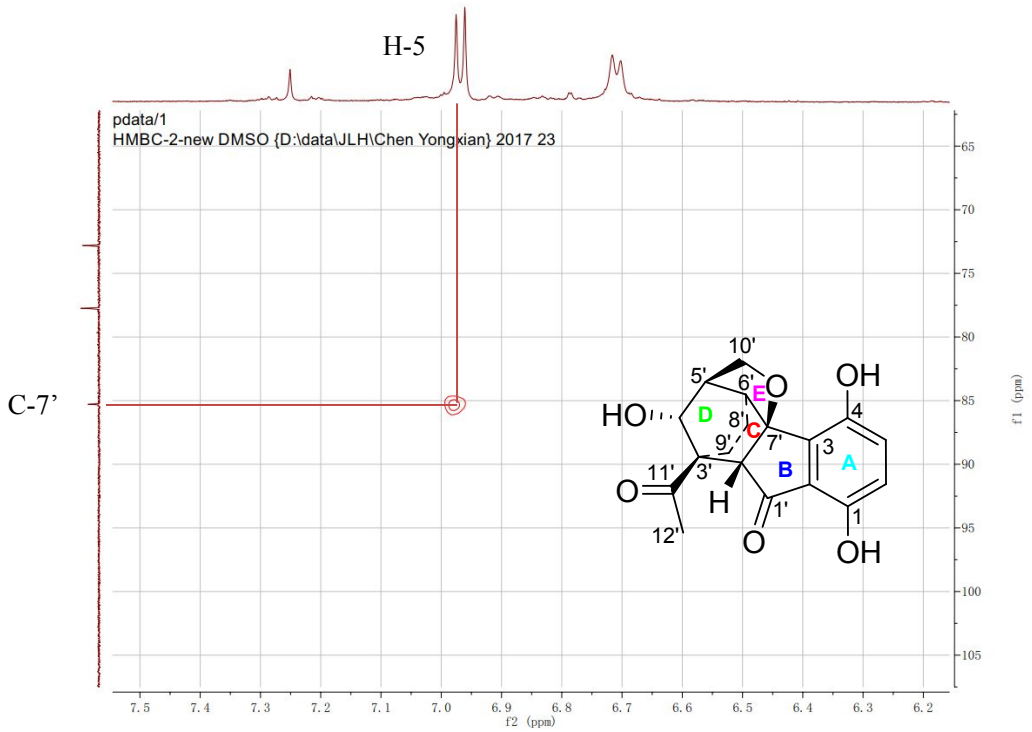

Figure S11. Partial HMBC spectrum of **1** in DMSO-d_6.

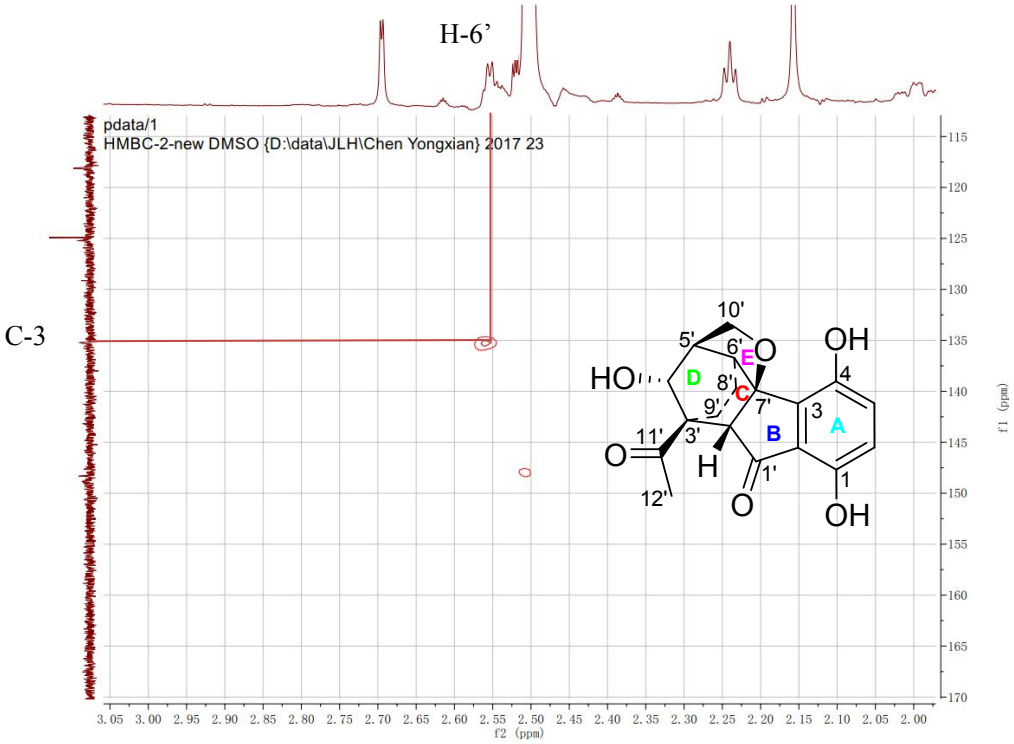

Figure S12. Partial HMBC spectrum of **1** in DMSO-d_6.

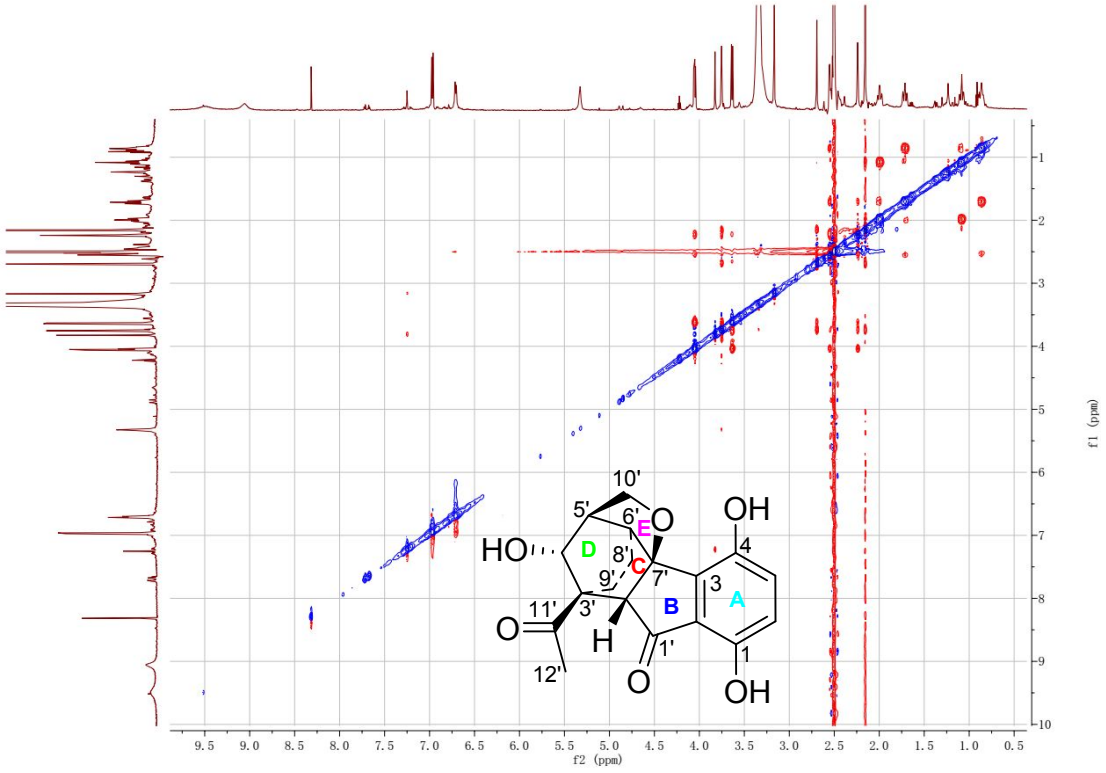

Figure S13. ROESY spectrum of **1** in DMSO-d_6.

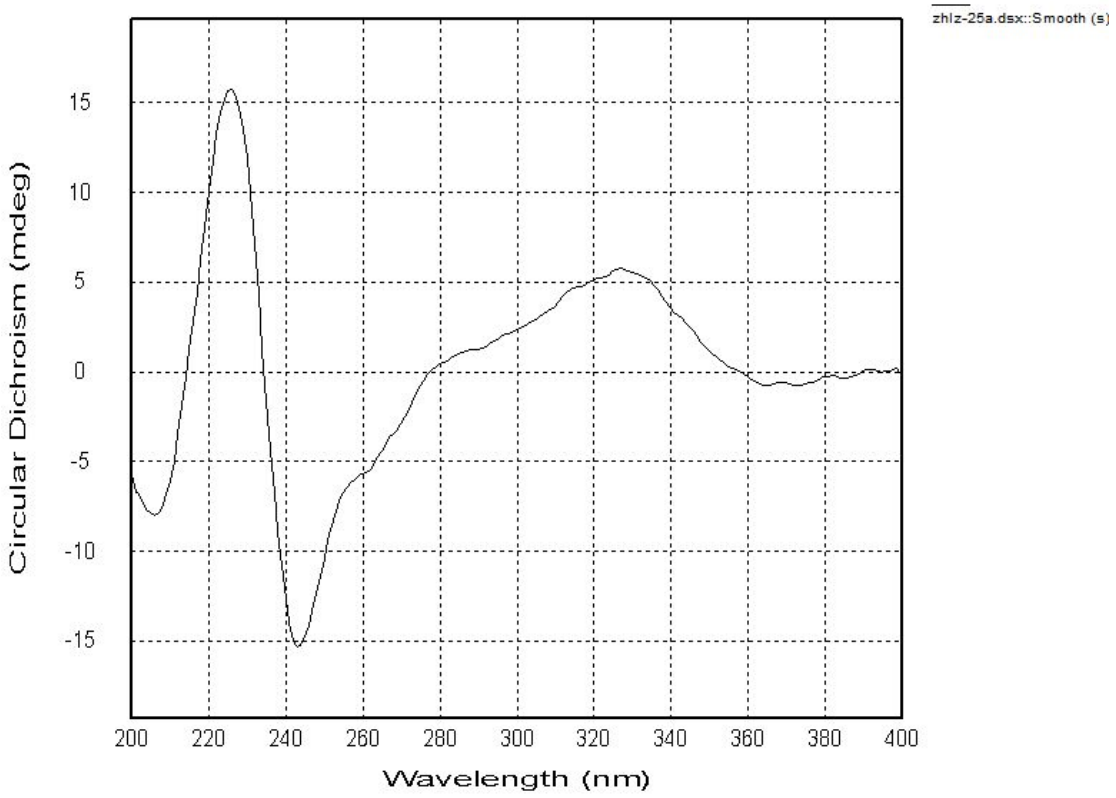

Figure S14. CD spectrum of (+)-**1** in MeOH.

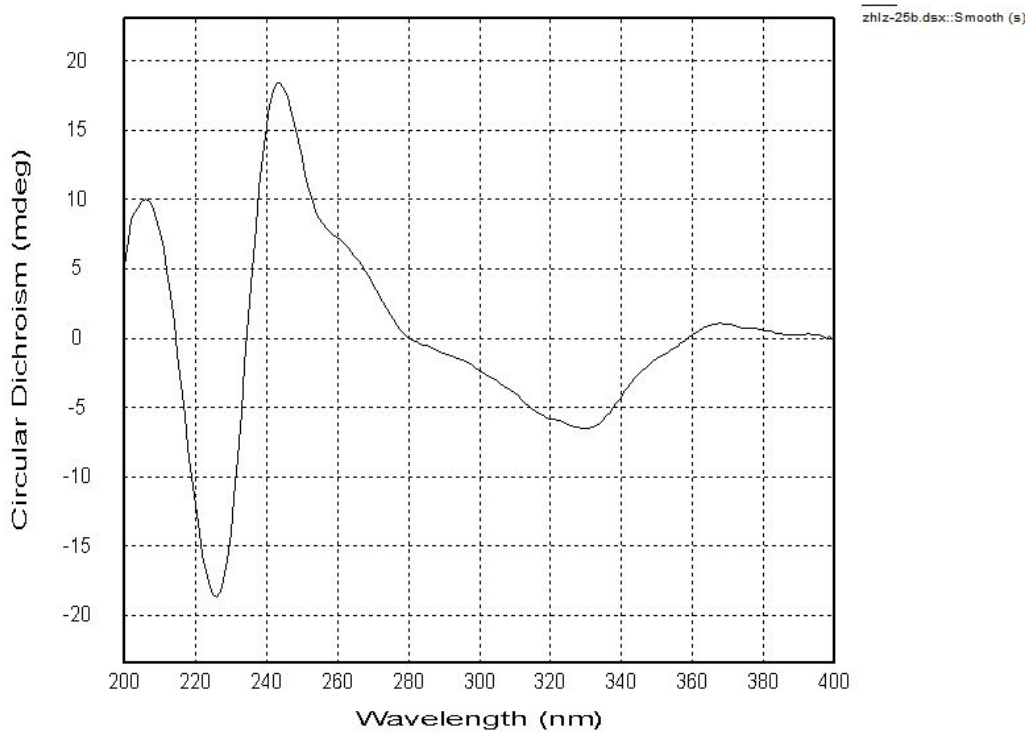

Figure S15. CD spectrum of (–)-**1** in MeOH.

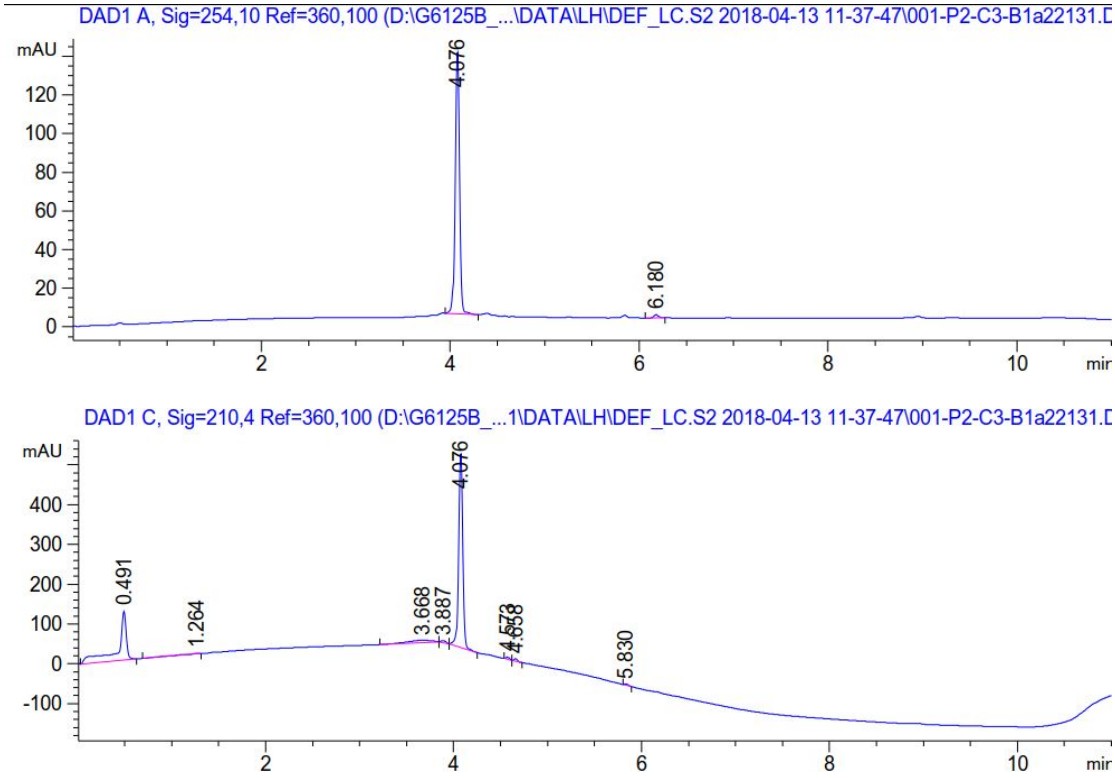

Figure S16. HPLC analysis of compound **1** (Acetonitrile/H_2O (CF_3COOH, 0.05%), 0-5 min, 10%-100%, 5-10 min, 100%; T=30 ℃; flow rate: 0.3 mL/min).

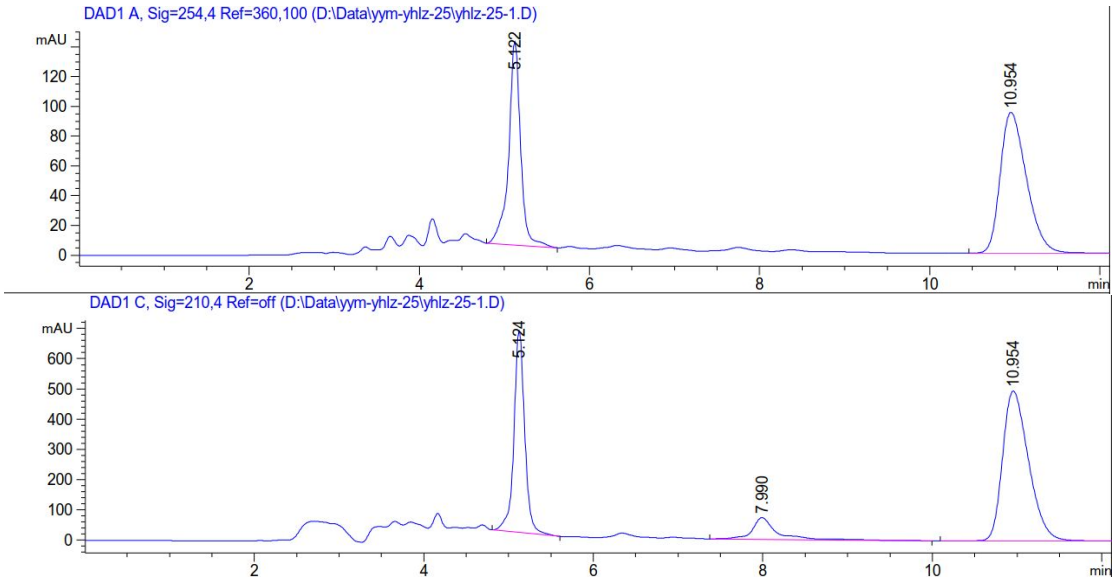

Figure S17. Chiral HPLC separation of racemic **1** (*n*-hexane/isopropanol, 68:32; T=30 ℃; flow rate: 1.0 mL/min; wavelength: 210 nm and 254 nm).

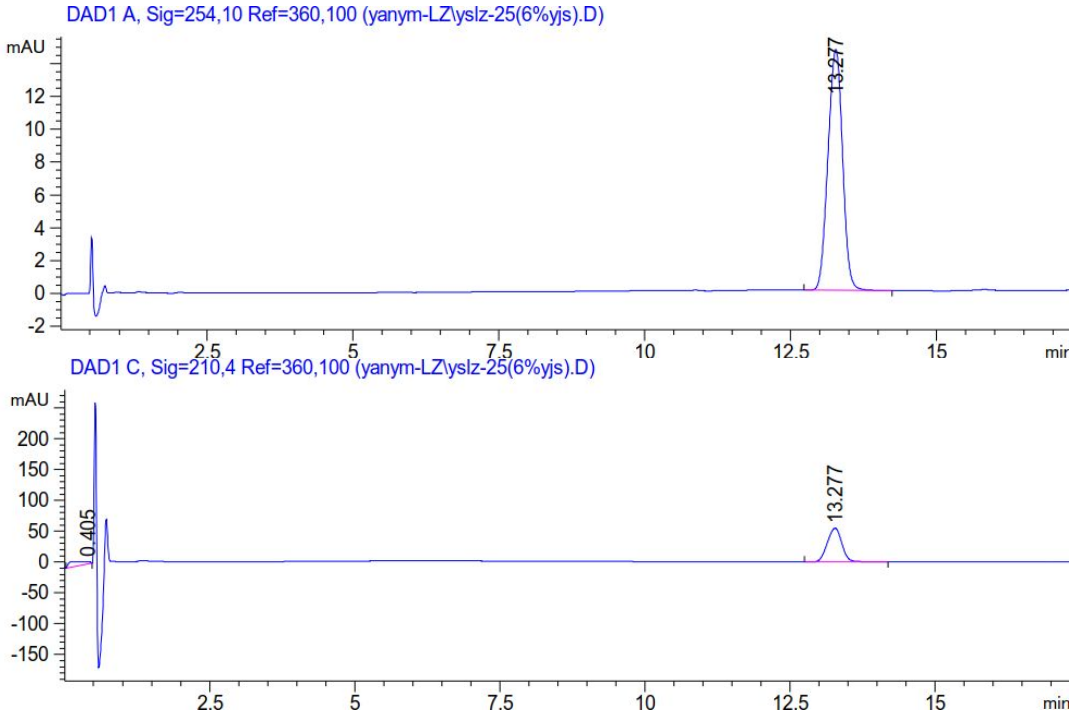

Figure S18. HPLC analysis of compound (–)-**1** for purity examination (Acetonitrile/H_2O (CF_3COOH, 0.05%), 6:94; T=30 ℃; flow rate: 0.3 mL/min; wavelength: 210 nm and 254 nm).

pubmed - "Cyclooxygenase 2"	
year	count
1992	4
1993	8
1994	30
1995	49
1996	140
1997	322
1998	406
1999	661
2000	833
2001	1082
2002	1366
2003	1473
2004	1698
2005	1802
2006	1982
2007	1871
2008	1703
2009	1756
2010	1789
2011	1755
2012	1785
2013	1831
2014	1807
2015	1714
2016	1621
2017	1569
2018	1491
2019	824

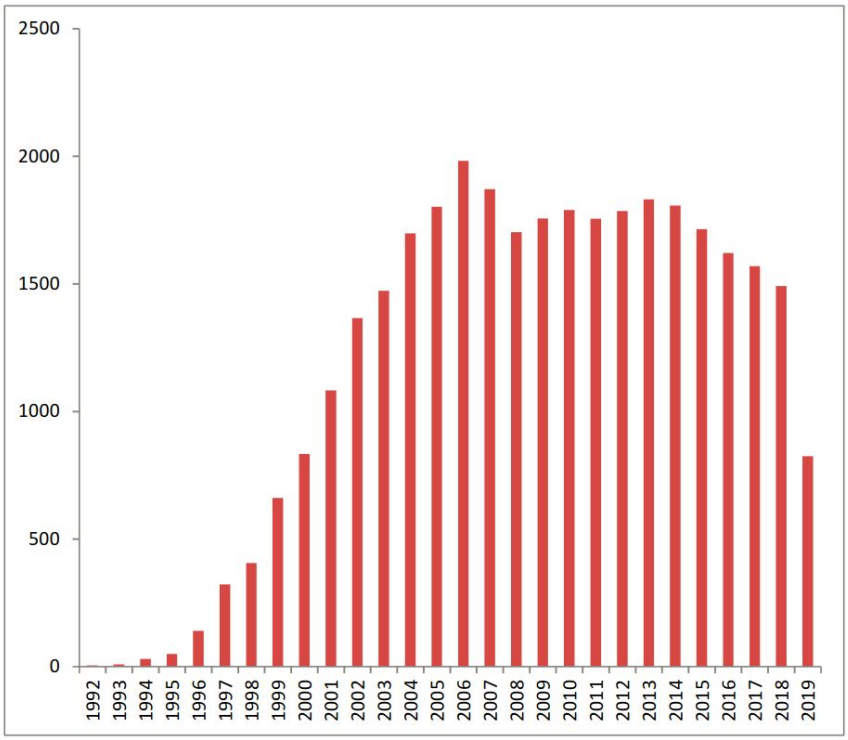

Figure S19. Research topic about 'COX-2' from PubMed during 1992–2019.

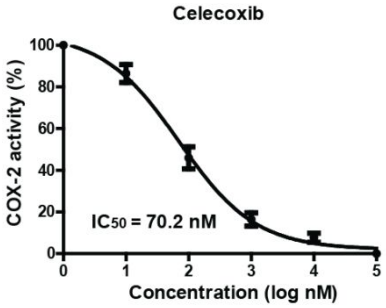

Figure S20. The IC_{50} value of celecoxib toward recombinant COX-2 was determined by plotting and analyzing the inhibition curve data using Graph Pad Prism 5 software (Mountain View, CA).

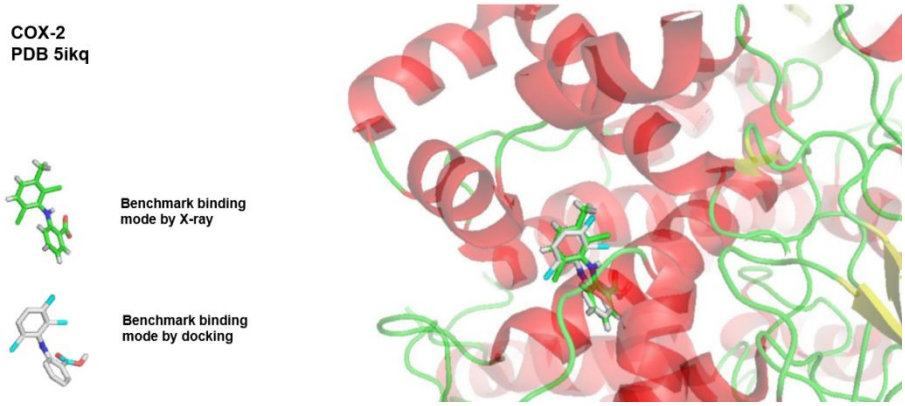

Figure S21. Molecular docking analysis illustrates the favorable binding positions of benchmark (meclofenamic acid) with lowest binding free energy in the catalytic site of human COX-2 (PDB code 5IKQ). The three-dimensional diagram shows the interactions of benchmark (green stick: experimental conformation; gray stick: predicted conformation) to human COX-2 (colored cartoon).

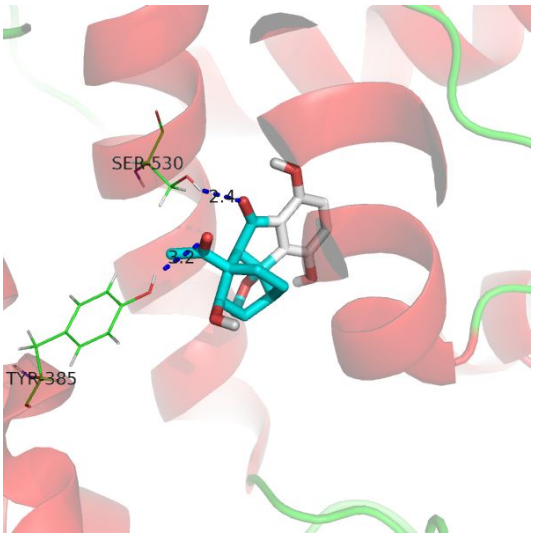

Figure S22. Molecular docking analysis illustrates the favorable binding positions of (+)-**1** with lowest binding free energy in the catalytic site of human COX-2 (PDB code 5IKQ). The three-dimensional diagram shows the interactions of (+)-**1** (cyan stick) to human COX-2 (red cartoon) with labeled residues (green line).

Detailed isolation procedures

1. General experimental procedures

Optical rotations were measured on a Bellingham + Stanley ADP 440 + digital polarimeter. UV spectrum was obtained on a Shimadzu UV-2600 spectrometer. CD spectra were recorded on a Chirascan instrument. NMR spectra were measured on a Bruker AV-600 spectrometer, with TMS as an internal standard. ESIMS was

collected on an Agilent G6125B LC/MSD spectrometer. HRESIMS was collected by a Shimazu LC-20AD AB SCIEX triple TOF 5600+ MS spectrometer. Silica gel (200−300 mesh; Qingdao Marine Chemical Inc., PR China), C-18 silica gel (40−60 μm; Daiso Co., Japan), MCI gel CHP 20P (75−150 μm, Mitsubishi Chemical Industries, Tokyo, Japan), and Sephadex LH-20 (Amersham Pharmacia, Sweden) were used for column chromatography. Semi-preparative HPLC equipment was a SEP LC-52 with a MWD UV detector (Separation Technology Co. Ltd., Beijing, PR China) equipped with an Agilent Zorbax SB-C_{18} column (250 mm × 9.4 mm, i.d., 5 μm). Chiral separation was carried out using an Agilent 1260 liquid chromatograph equipped with a Daicel Chiralpak AD-H column (250 mm × 4.6 mm, i.d., 5 μm).

2. Fungal material

The fruiting bodies of *G. lucidum* cultivated in Yongsheng County of Yunnan Province were purchased from Tongkang Pharmaceutical Co. Ltd. in Guangzhou Province, PR China, in December 2017. The material was identified by Prof. Zhu-Liang Yang at Kunming Institute of Botany, Chinese Academy of Sciences, PR China, and a voucher specimen (CHYX-0609) was deposited at School of Pharmaceutical Sciences, Shenzhen University Health Science Center, PR China.

3. Extraction and isolation

The fruiting bodies of *G. lucidum* (40 kg) were powdered and extracted by diacolation method with 95% EtOH (flow rate: 3 mL/min; 480 L in total) at room temperature. After removal of solvents under reduced pressure, a crude extract (1.7 kg) was obtained, which was suspended in H_2O and partitioned with EtOAc three times to afford an EtOAc extract (1.3 kg). This extract was subjected to a MCI gel CHP 20P column with gradient aqueous MeOH (40%–100%) to get nine fractions (Fr.A–Fr.I). Fr.B (14.1 g) was submitted to Sephadex LH-20 (MeOH) to yield three fractions (Fr.B.1–Fr.B.3). Fr.B.2 (6.4 g) was submitted to a RP-18 column eluted with aqueous MeOH (30%–100%) to produce seven fractions (Fr.B.2.1–Fr.B.2.7). Among them, Fr.B.2.1 (1.97 g) was gel filtrated on Sephadex LH-20 (MeOH) to afford two fractions (Fr.B.2.1.1–Fr.B.2.1.2). Fr.B.2.1.2 (1.4 g) was isolated by MCI gel CHP 20P column with gradient aqueous MeOH (25%–100%) to get six fractions (Fr.B.2.1.2.1–Fr.B.2.1.2.6). Further purification of Fr.B.2.1.2.2 (420 mg) by Sephadex LH-20

(MeOH) and semi-preparative HPLC eluted with aqueous acetonitrile (15%) afforded compound **1** (1.8 mg, t_R = 28.1 min, flow rate: 3 mL/min). Compound **1** is a racemate which was submitted to semi-preparative HPLC on a chiral phase (*n*-hexane/isopropanol, 68:32, flow rate: 1.0 mL/min) to afford (+)-**1** (0.4 mg, t_R = 5.1 min) and (−)-**1** (0.6 mg, t_R = 10.9 min), respectively.

X-ray crystallographic data

Crystal data for (−)-**1**: $C_{18}H_{18}O_6$ (M =330.32 g/mol), monoclinic, space group $P2_1$ (no. 4), a = 10.1710(3) Å, b = 7.5398(2) Å, c = 10.1710(3) Å, β = 110.85°, V = 728.89(4) Å^3, Z = 2, T = 100.0 K, μ(CuKα) = 0.948 mm^{-1}, *Dcalc* = 1.505 g/cm^3, 11742 reflections measured (10.562° ≤ 2θ≤ 136.802°), 2625 unique (R_{int} = 0.0252, R_{sigma} = 0.0201) which were used in all calculations. The final R_1 was 0.0251 (I > 2σ(I)) and wR_2 was 0.0651 (all data).

Table S2. Crystal data and structure refinement for (−)-1.

Identification code	cxy0429 [(−)-**1**]
Empirical formula	$C_{18}H_{18}O_6$
Formula weight	330.32
Temperature/K	100.0
Crystal system	monoclinic
Space group	$P2_1$
a/Å	10.1710(3)
b/Å	7.5398(2)
c/Å	10.1710(3)
α/°	90
β/°	110.85
γ/°	90
Volume/Å^3	728.89(4)
Z	2
ρ_{calc}g/cm^3	1.505
μ/mm^{-1}	0.948
F(000)	348.0
Crystal size/mm^3	0.30 × 0.30 × 0.18
Radiation	CuKα (λ = 1.54178)
2θ range for data collection/°	10.562 to 136.802
Index ranges	-12 ≤ h ≤ 11, -9 ≤ k ≤ 9, -12 ≤ l ≤ 12
Reflections collected	11742
Independent reflections	2625 [R_{int} = 0.0252, R_{sigma} = 0.0201]
Data/restraints/parameters	2625/1/222
Goodness-of-fit on F^2	1.045
Final R indexes [I>=2σ (I)]	R_1 = 0.0251, wR_2 = 0.0649

Final R indexes [all data]	R_1 = 0.0254, wR_2 = 0.0651
Largest diff. peak/hole / e Å^{-3}	0.19/-0.14
Flack parameter	0.03(6)

Table S3. Fractional Atomic Coordinates (×10^4) and Equivalent Isotropic Displacement Parameters (Å^2×10^3) for (−)-1. U_{eq} is defined as 1/3 of of the trace of the orthogonalised U_{IJ}tensor.

Atom	*x*	*y*	*z*	U(eq)
O1	3293.2(15)	5388(2)	9525.6(14)	21.6(3)
O2	4753.6(13)	6682.0(19)	5838.0(13)	17.7(3)
O3	2155.6(14)	1381.6(19)	4874.6(14)	18.7(3)
O4	2868.1(15)	8760.1(18)	3133.6(15)	20.2(3)
O5	987.2(14)	1835.7(18)	1803.4(14)	19.5(3)
O6	4307.1(15)	1405(2)	8259.5(15)	23.1(3)
C1	1171(2)	4829(3)	1146(2)	17.7(4)
C2	1425(2)	3534(3)	2177.5(19)	16.2(4)
C3	2147.6(19)	4035(3)	3571.8(19)	14.9(4)
C4	2518.8(19)	2917(3)	4827.7(19)	14.2(4)
C5	3414.3(19)	4018(3)	6076.7(18)	14.8(4)
C6	2912.9(19)	3946(3)	7337.7(18)	14.5(4)
C7	3166(2)	2109(3)	8011.0(18)	17.1(4)
C8	2038(2)	1245(3)	8419(2)	27.5(5)
C9	3870.7(19)	5252(3)	8444.8(19)	16.3(4)
C10	3914(2)	7064(3)	7744.1(19)	17.0(4)
C11	2702(2)	7161(3)	6310.2(19)	16.2(4)
C12	3362.5(19)	5944(2)	5508(2)	14.6(4)
C13	5192(2)	7295(3)	7293.0(19)	19.2(4)
C14	2637.8(19)	5768(3)	3939.6(19)	14.8(4)
C15	2409.6(19)	7031(3)	2894(2)	16.4(4)
C16	1666.5(19)	6543(3)	1505(2)	17.7(4)
C17	1283.7(19)	6514(3)	6311(2)	18.1(4)
C18	1383(2)	4608(3)	6880.2(19)	15.9(4)

Table S4. Anisotropic Displacement Parameters (Å^2×10^3) for (−)-1. The Anisotropic displacement factor exponent takes the form: -2π^2[h^{2}a*^{2}U$_{11}$+2hka*b*U$_{12}$+…].

Atom	U_{11}	U_{22}	U_{33}	U_{23}	U_{13}	U_{12}
O1	21.8(7)	31.7(8)	12.5(6)	-5.5(6)	7.5(5)	-7.0(6)
O2	15.5(6)	22.6(7)	16.3(6)	-3.5(6)	7.3(5)	-5.3(5)
O3	22.3(7)	15.3(7)	18.4(7)	0.0(5)	7.3(5)	0.3(5)
O4	26.4(7)	16.0(7)	17.8(7)	0.8(5)	7.5(6)	-1.5(6)
O5	24.0(7)	17.2(8)	15.5(6)	-1.1(5)	4.7(5)	-2.5(6)

O6	21.6(7)	23.3(8)	20.8(7)	4.0(6)	3.2(5)	4.4(6)
C1	16.0(9)	25.0(11)	12.3(9)	-0.6(8)	5.2(7)	2.1(8)
C2	14.4(9)	18.8(10)	16.5(9)	-2.0(8)	7.0(8)	0.5(7)
C3	14.4(8)	16.9(9)	14.5(9)	0.9(8)	6.7(7)	0.6(7)
C4	13.5(9)	16.4(10)	13.6(9)	-1.1(7)	6.1(7)	2.6(7)
C5	14.1(8)	16.6(9)	14.1(9)	0.6(7)	5.6(7)	1.8(7)
C6	14.4(9)	16.7(9)	11.9(8)	-0.2(7)	4.1(7)	-0.8(7)
C7	21.0(10)	19.4(10)	10.1(8)	-0.5(7)	4.4(7)	1.1(8)
C8	34.8(11)	19.5(10)	36.2(12)	6.8(9)	22.3(10)	2.7(9)
C9	14.7(8)	21.6(10)	12.1(9)	-1.5(8)	4.0(7)	-0.7(8)
C10	18.1(9)	17.8(10)	15.5(9)	-3.2(8)	6.5(7)	-2.7(8)
C11	18.1(9)	14.8(9)	16.2(9)	-1.2(7)	7.0(7)	-0.2(8)
C12	14.1(9)	15.0(9)	14.4(9)	0.4(7)	4.8(7)	-1.3(7)
C13	18.8(9)	22.2(10)	17.0(9)	-5.1(8)	7.0(8)	-6.4(8)
C14	14.1(8)	17.5(10)	14.4(9)	-1.1(7)	7.2(7)	1.1(7)
C15	16.3(9)	16.0(9)	18.7(9)	1.0(8)	8.6(7)	2.3(8)
C16	17.9(8)	21.3(10)	15.8(9)	4.7(8)	8.4(7)	3.9(8)
C17	15.8(9)	19.8(10)	19.6(9)	1.2(8)	7.2(7)	2.9(8)
C18	14.2(9)	18.2(10)	15.6(9)	-2.4(8)	5.4(7)	-1.7(7)

Table S5. Bond Lengths for (−)-1.

Atom	Atom	Length/Å	Atom	Atom	Length/Å
O1	C9	1.423(2)	C5	C12	1.557(3)
O2	C12	1.444(2)	C6	C7	1.526(3)
O2	C13	1.460(2)	C6	C9	1.551(3)
O3	C4	1.221(2)	C6	C18	1.540(3)
O4	C15	1.377(3)	C7	C8	1.501(3)
O5	C2	1.364(2)	C9	C10	1.549(3)
O6	C7	1.218(2)	C10	C11	1.540(3)
C1	C2	1.388(3)	C10	C13	1.535(3)
C1	C16	1.388(3)	C11	C12	1.533(3)
C2	C3	1.397(3)	C11	C17	1.523(3)
C3	C4	1.463(3)	C12	C14	1.506(3)
C3	C14	1.401(3)	C14	C15	1.384(3)
C4	C5	1.519(3)	C15	C16	1.393(3)
C5	C6	1.541(2)	C17	C18	1.539(3)

Table S6. Bond Angles for (−)-1.

Atom	Atom	Atom	Angle/°	Atom	Atom	Atom	Angle/°
C12	O2	C13	106.13(13)	O1	C9	C10	112.26(16)
C16	C1	C2	120.27(17)	C10	C9	C6	109.83(15)

O5	C2	C1	119.67(17)	C11	C10	C9	109.48(15)
O5	C2	C3	122.57(17)	C13	C10	C9	113.78(16)
C1	C2	C3	117.75(18)	C13	C10	C11	100.89(15)
C2	C3	C4	127.54(18)	C12	C11	C10	96.96(15)
C2	C3	C14	122.13(17)	C17	C11	C10	115.03(15)
C14	C3	C4	110.32(16)	C17	C11	C12	113.79(16)
O3	C4	C3	126.33(18)	O2	C12	C5	111.85(15)
O3	C4	C5	125.79(17)	O2	C12	C11	102.96(14)
C3	C4	C5	107.87(16)	O2	C12	C14	110.47(14)
C4	C5	C6	113.53(15)	C11	C12	C5	108.89(15)
C4	C5	C12	105.54(15)	C14	C12	C5	104.50(15)
C6	C5	C12	111.39(15)	C14	C12	C11	118.34(15)
C5	C6	C9	105.88(15)	O2	C13	C10	106.36(14)
C7	C6	C5	110.64(15)	C3	C14	C12	111.01(16)
C7	C6	C9	106.75(14)	C15	C14	C3	119.35(17)
C7	C6	C18	114.90(16)	C15	C14	C12	129.65(17)
C18	C6	C5	109.60(14)	O4	C15	C14	124.18(17)
C18	C6	C9	108.64(15)	O4	C15	C16	117.18(17)
O6	C7	C6	119.03(18)	C14	C15	C16	118.64(18)
O6	C7	C8	121.26(19)	C1	C16	C15	121.83(18)
C8	C7	C6	119.64(17)	C11	C17	C18	111.33(15)
O1	C9	C6	106.35(15)	C17	C18	C6	109.89(15)

Table S7. Torsion Angles for (−)-1.

A	B	C	D	Angle/°	A	B	C	D	Angle/°
O1	C9	C10	C11	-102.62(17)	C7	C6	C9	C10	168.15(15)
O1	C9	C10	C13	145.36(16)	C7	C6	C18	C17	176.23(15)
O2	C12	C14	C3	126.65(16)	C9	C6	C7	O6	-67.6(2)
O2	C12	C14	C15	-53.7(2)	C9	C6	C7	C8	109.4(2)
O3	C4	C5	C6	-48.4(2)	C9	C6	C18	C17	56.77(19)
O3	C4	C5	C12	-170.68(18)	C9	C10	C11	C12	-75.51(17)
O4	C15	C16	C1	179.26(17)	C9	C10	C11	C17	44.9(2)
O5	C2	C3	C4	-1.8(3)	C9	C10	C13	O2	91.64(18)
O5	C2	C3	C14	177.59(17)	C10	C11	C12	O2	-50.40(16)
C1	C2	C3	C4	179.28(17)	C10	C11	C12	C5	68.44(18)
C1	C2	C3	C14	-1.4(3)	C10	C11	C12	C14	-172.53(16)
C2	C1	C16	C15	-0.8(3)	C10	C11	C17	C18	-55.5(2)
C2	C3	C4	O3	-6.3(3)	C11	C10	C13	O2	-25.5(2)
C2	C3	C4	C5	174.87(18)	C11	C12	C14	C3	-115.10(19)
C2	C3	C14	C12	179.36(16)	C11	C12	C14	C15	64.6(3)
C2	C3	C14	C15	-0.3(3)	C11	C17	C18	C6	2.3(2)
C3	C4	C5	C6	130.39(16)	C12	O2	C13	C10	-6.2(2)
C3	C4	C5	C12	8.12(18)	C12	C5	C6	C7	-171.93(15)

C3	C14	C15	O4	-178.71(16)	C12	C5	C6	C9	-56.63(19)
C3	C14	C15	C16	1.5(3)	C12	C5	C6	C18	60.36(19)
C4	C3	C14	C12	-1.2(2)	C12	C11	C17	C18	55.1(2)
C4	C3	C14	C15	179.10(16)	C12	C14	C15	O4	1.7(3)
C4	C5	C6	C7	69.1(2)	C12	C14	C15	C16	-178.15(17)
C4	C5	C6	C9	-175.61(16)	C13	O2	C12	C5	-80.80(18)
C4	C5	C6	C18	-58.6(2)	C13	O2	C12	C11	35.96(18)
C4	C5	C12	O2	-128.05(15)	C13	O2	C12	C14	163.24(15)
C4	C5	C12	C11	118.83(15)	C13	C10	C11	C12	44.72(18)
C4	C5	C12	C14	-8.52(18)	C13	C10	C11	C17	165.09(16)
C5	C6	C7	O6	47.2(2)	C14	C3	C4	O3	174.25(18)
C5	C6	C7	C8	-135.84(17)	C14	C3	C4	C5	-4.5(2)
C5	C6	C9	O1	171.93(15)	C14	C15	C16	C1	-0.9(3)
C5	C6	C9	C10	50.23(19)	C16	C1	C2	O5	-177.06(17)
C5	C6	C18	C17	-58.48(19)	C16	C1	C2	C3	1.9(3)
C5	C12	C14	C3	6.2(2)	C17	C11	C12	O2	-171.71(15)
C5	C12	C14	C15	-174.15(19)	C17	C11	C12	C5	-52.9(2)
C6	C5	C12	O2	108.31(17)	C17	C11	C12	C14	66.2(2)
C6	C5	C12	C11	-4.8(2)	C18	C6	C7	O6	171.92(16)
C6	C5	C12	C14	-132.16(15)	C18	C6	C7	C8	-11.1(2)
C6	C9	C10	C11	15.5(2)	C18	C6	C9	O1	54.29(19)
C6	C9	C10	C13	-96.54(18)	C18	C6	C9	C10	-67.41(19)
C7	C6	C9	O1	-70.14(18)					

Table S8. Hydrogen Atom Coordinates (Å×10^4) and Isotropic Displacement Parameters (Å^2×10^3) for (−)-1.

Atom	*x*	*y*	*z*	U(eq)
H1	3901.91	5803.03	10256.15	32
H4	3351.11	8893.63	3990.01	30
H5	1344.88	1161.11	2496.64	29
H1A	657.09	4540.76	191.42	21
H5A	4406.65	3581.38	6387.31	18
H8A	2346.84	57.36	8792.79	41
H8B	1174.09	1152.58	7590.83	41
H8C	1857.83	1962.39	9140.76	41
H9	4844.18	4754.3	8846.12	20
H10	3852.15	8062.96	8366.6	20
H11	2613.57	8394.21	5926.26	19
H13A	5479.41	8556.01	7359.7	23
H13B	5995.44	6583.15	7903	23
H16	1494.04	7408.17	783.82	21
H17A	586.78	6554.8	5340.35	22
H17B	953.25	7313.94	6901.25	22

H18A	762.66	3818.96	6140.76	19
H18B	1064.22	4580.17	7693.17	19

Biological Assays

Biological Assays of Compounds (+)-1 and (–)-1

1. Expression and purification of human recombinant COX-1 and COX-2 in *Escherichia coli*

Human COX-1/COX-2 protein-encoding sequence (without signal peptide) were subcloned into the pET-30a constructs. All COX-2 mutants (Y385A, S530A) were generated by site-directed mutagenesis and confirmed by sequencing. The wild type and mutant recombinant proteins were purified with Ni-ATA column after IPTG induction at 18℃ for 24 hours.

2. In vitro cyclooxygenase (COX) inhibitory assay

Compounds were evaluated for COX inhibitory activity in vitro by using Cayman's COX Fluorescent Inhibitor Screening Assay Kit (Cayman hemical Company, Ann Arbor, MI, USA). Human recombinant COX-1/COX-2 enzyme were pre-incubated with serially diluted test compounds for 15 min at room temperature, heme and fluorometric substrate were added and incubated for another 15 min at room temperature. The reaction was started by the addition of arachidonic acid and allowed to proceed for 2 min. The intensity of fluorescence was measured using a 530 nm excitation wavelength and a 595 nm emission wavelength using a micro plate reader (BioTek).The data were analyzed using GraphPad Prism5 (GraphPad SoftwareInc.). All the tests were performed in triplicate.

3. IC_{50} evaluation based on the non-linear regression

We developed the IC_{50} assay strictly following the user's manual of the Graphpad Prism software package (Mountain View, CA), which has been chosen as the protocol for IC_{50} evaluation by numerous published studies. Briefly, the compounds were serial diluted and added to the reaction mixture for incubation. The corresponding enzyme activity were recorded and normalized as the percentage of the full enzyme activity of COX-1/COX-2. Afterwards, the dose-response curve were generated based

on the nonlinear regression fitting of log-transformed data of serial diluted concentration value (X axis value) and the normalized enzyme activity data (Y axis value). During this procedure, the standard equation "log(inhibitor) vs. response -- Variable slope (four parameters)", a built-in module of the GraphPad Prism5 software Package (Mountain View, CA) was employed to made the curve fitting and IC_{50} calculation. All the tests were performed in triplicate.

4. Statistics

Data are expressed as means ± standard error of the mean (SEM) of the indicated independent experiments. Statistical analyses were performed by Student's t-test or One-Way Analysis of Variance (ANOVA) by a post-hoc test. * $p < 0.05$ was considered significant.

Docking study

For ligand preparation, compounds (+)-**1** and (–)-**1** were drawn and converted to PDB format by CORINA online service (http://www.molecular-networks.com/online demos/corinademo/). The PDB format of ligand was then converted to PDBQT format by AutoDock Tools 1.5.6 (The Scripps Research Institute, CA, USA). For receptor preparation, 5IKQ human COX-2 models was downloaded from Protein Data Bank. Both ligands and water molecules in 5IKQ were removed by Chimera 1.7mac (UCSF Resource for Biocomputing, Visualization, and Informatics, CA, USA). The modified 5IKQ was converted to PDBQT format by AutoDock Tools 1.5.6 (The Scripps Research Institute, CA, USA) with minor modifications.

The software AutoDock Vina v.1.0.2 (downloadable at http://vina.scripps.edu/) developed in the Molecular Graphics Lab at The Scripps Research Institute (Trott & Olson, 2010) was used for all dockings in this study. The docking parameters for AutoDock Vina were kept to their default values. The grid box was 20 Å × 20 Å × 18 Å, encompassing the catalytic cavity of COX-2. The binding modes were clustered through the root-mean square deviation (RMSD) among the Cartesian coordinates of the ligand atoms. The binding modes with lowest binding free energy and the most cluster members were chosen for the optimum docking conformation. The binding mode were illustrated by PyMOL Molecular Graphics System Version 1.3 (Schrödinger, LLC).

To validate our docking model, we extracted the inhibitors from the original protein model. Our docking simulation showed that the predicted conformations of the inhibitor is close to the experimental conformations of the inhibitor. Furthermore, the inhibitor exhibited a high binding score (−8.6 kcal/mol) against human COX-2 (Figure S21).